



**The Impact of Cation and Anion Pairing in Ionic Salts on  
Surface Defect Passivation in Cesium Lead Bromide  
Nanocrystals**

|                               |  |
|-------------------------------|--|
| Journal:                      | <i>Journal of Materials Chemistry C</i>  |
| Manuscript ID                 | TC-ART-09-2020-004257.R2   |
| Article Type:                 | Paper  |
| Date Submitted by the Author: | 25-Nov-2020  |
| Complete List of Authors:     | Yoon, Lucy; University of Virginia, Chemical Engineering<br>Alpert, Matthew; University of Virginia, Department of Chemical Engineering<br>Luo, Hongxi; University of Virginia, Department of Chemical Engineering<br>Schapowal, Michael; University of Virginia, Department of Chemical Engineering<br>Holmgren, Eric; University of Virginia, Department of Chemical Engineering<br>Geise, Geoffrey; University of Virginia, Department of Chemical Engineering<br>Paolucci, Christopher; University of Virginia, Department of Chemical Engineering<br>Choi, Joshua; University of Virginia, Department of Chemical Engineering |
|                               |  |

## ARTICLE

## The Impact of Cation and Anion Pairing in Ionic Salts on Surface Defect Passivation in Cesium Lead Bromide Nanocrystals

Received 00th January 20xx,  
Accepted 00th January 20xx

Lucy U. Yoon, Matthew R. Alpert, Hongxi Luo, Michael I. Schapowal, Eric Holmgren, Geoffrey M. Geise, Christopher Paolucci, Joshua J. Choi\*

DOI: 10.1039/x0xx00000x

Imperfect passivation of surface charge traps on metal halide perovskite (MHP) nanocrystals remains a key obstacle to achieving higher performance in optoelectronic devices. Due to the strong ionic nature of MHPs, ionic salts have been identified as effective surface charge trap passivating ligands. In this study, based on photoluminescence quantum yield (PLQY) and time-resolved photoluminescence (TRPL) measurements on cesium lead bromide nanocrystals (CsPbBr<sub>3</sub> NCs), we find that the pairing between cation and anion of an ionic salt results in a significant impact on trap passivation. Using density of functional theory (DFT) calculations, we identify the binding interaction between the cation and anion of the ionic pair to be a major factor in determining the trap passivation efficacy.

### Introduction

Metal halide perovskites (MHPs) are promising semiconductors for a wide variety of optoelectronic applications including photovoltaics, light-emitting diodes (LEDs), photodetectors, and lasers.<sup>1-6</sup> MHPs combine superb optical and electrical properties with the possibility of low-cost solution based manufacturing.<sup>3, 7-15</sup> Properties of MHPs such as the widely tunable bandgap, narrow full-width-half-maximum (FWHM) emissions, and bright photoluminescence (PL) with a versatility of low-temperature processing conditions<sup>16-19</sup> are essential features for the advancement of (LED) technology, which requires highly saturated color displays, lower manufacturing costs, and high quantum efficiency.<sup>20-23</sup> Among the various MHPs, cesium lead halide perovskites (CsPbX<sub>3</sub>) are promising for practical device applications due to their intrinsic stability<sup>16, 24-28</sup> and defect-tolerant nature. In particular, CsPbBr<sub>3</sub> nanocrystals (NCs) have shown superior optical properties including near-unity photoluminescence quantum yield (PLQY),<sup>29, 30</sup> sharp PL emission peak,<sup>31</sup> and a highly saturated color emission. Recently, CsPbBr<sub>3</sub> NCs-based LEDs have shown encouraging progress with their performance exceeding an external quantum efficiency (EQE) of 16%.<sup>32</sup>

Despite the promising potentials, a further increase in the performance of MHP NC-based optoelectronic devices is currently limited by non-radiative electron-hole recombination at trap sites on the NC surfaces.<sup>33-39</sup> One facile yet effective solution to this challenge is a post-synthesis surface treatment with trap passivating ligand molecules.<sup>40-47</sup> Depending on the nature of defect sites on the surface, various types of ligands<sup>31,</sup>

<sup>48</sup> can be employed to improve trap passivation. Charge neutral Lewis base L-type ligands bind with a Lewis acid site on the NC surface by donating an electron pair. Conversely, charge neutral Lewis acid Z-type ligands bind with a Lewis base on the NC surface by accepting an electron pair. Due to a strong ionic nature of MHP surface, ionic salts<sup>47, 49-53</sup> recently have been studied as trap passivating ligands. Cation and anion of ionic salts behave as charged X-type ligands which passivate charge traps by either donating or accepting an electron to under-coordinated surface atoms. Despite all of the studies so far, precise mechanisms through which ligands and MHP surface interact are still not well understood and methods of selecting effective ligand species for particular MHP surfaces remain elusive.

In order to optimize MHP NC surface – ligand interactions for superior charge trap passivation, the surface environment and the defect properties of NCs must be understood. A collection of studies<sup>53, 54</sup> on Pb-based MHPs has reported that a majority of the detrimental surface charge traps is based on halide vacancies. In order to eradicate these detrimental defects, exposed Pb<sup>2+</sup>, an under-coordinated atom due to absence of halides, needs to be coordinated with a counterion. As such, finding an anion with effective binding affinity to Pb<sup>2+</sup> is an essential aspect to improving charge trap passivation. One study recently proposed that the Lewis basicity of anion in ionic salt plays a crucial role in trap passivation and used Hard-Soft Acid-Base theory as a guiding principle to discover that soft Lewis base anion binds best with soft Lewis acid Pb<sup>2+</sup> via coordinative bonding.<sup>53</sup>

While halide vacancies serve as detrimental trap sites and appear to have the most eminent effect on non-radiative recombination, other vacancies, such as monovalent cations are still present. Yet, computational studies<sup>54, 55</sup> suggest that their defect energy levels are likely to either lie outside of the MHP bandgap or are too shallow to serve as significant charge traps.

<sup>a</sup> Department of Chemical Engineering, University of Virginia, Charlottesville, Virginia 22904, United States

\*Corresponding Author: jjc6z@virginia.edu

Electronic Supplementary Information (ESI) available. See DOI: 10.1039/x0xx00000x

For that reason, the choice of cation and the cation – anion pairing have not yet been carefully taken into consideration when selecting an ionic pair as charge passivating ligands. Although passivation *via* binding of cations directly onto the MHP surface may not directly result in any significant charge trap passivation, we believe that the dissociation ability of the cation – anion pair into ionic species will be an important factor as ionic salts need to initially dissociate into ions for them to act as X-type ligands. Therefore, we hypothesize that the binding affinity of cation and anion pairing has a significant impact on surface charge trap passivation in MHP NCs.

Here, we study the relationship between cation-anion pairing in ionic salts and their efficacy in passivating surface charge traps in CsPbBr<sub>3</sub> NCs. CsPbBr<sub>3</sub> is the most widely studied composition in MHP NC field and is a great model system for this work. Our PLQY and PL lifetime results show that, given the identical anions, their pairing with different cations has a major impact on the degree of surface trap passivation. Our systematic comparison across different cation and anion pairs shows that certain anions can passivate traps well regardless of cations while other anions require pairing with specific cations for effective trap passivation. Using density functional theory (DFT) calculations, we identify the varying interaction energies of the cation – anion pair combinations to be a major factor resulting in the observed differences in trap passivation efficacy.

## Experimental

### Materials and methods

**Materials.** Cesium carbonate (Cs<sub>2</sub>CO<sub>3</sub>, 99.9%), octadecene (ODE, 90%), oleic acid (HOA, >99%), oleylamine (OLAm, 70%), anhydrous dimethyl sulfoxide (DMSO, 99.9%) were purchased from Sigma-Aldrich. Lead bromide (PbBr<sub>2</sub>, >99.99%) was purchased from TCI America. Cesium bromide (CsBr, >99.999%) was purchased from Alfa Aesar. Tetrabutylammonium bromide (TeBA<sub>4</sub>Br, >98%), tributylamine (>99%), dibutylamine (>99.5%), n-butylamine (99.5%), acetic acid (>99.85%), benzoic acid (>99.5%), difluoroacetic acid (98%), hydrobromic acid (HBr, 48%), and tetrabutylammonium hydroxide solution (TeBA<sub>4</sub>OH, 40 wt.% in H<sub>2</sub>O) were purchased from Sigma-Aldrich and used as received.

**Cesium oleate (Cs-oleate) synthesis.** Using Schlenk line setup, 0.407 g of Cs<sub>2</sub>CO<sub>3</sub>, 20 mL of ODE, 1.25 mL of HOA were placed in 100 mL three neck round flask. Under vacuum, the flask was heated at 120 °C for 1 hour to evaporate mostly water and impurities. Under Argon, the temperature was heated to 150 °C and solution was stirred until all Cs<sub>2</sub>CO<sub>3</sub> is dissolved. The final concentration of Cs-oleate is approximately 0.12 M. The final product needs to be heated prior to use as it often precipitates at room temperature.

**CsPbBr<sub>3</sub> NCs synthesis.** 0.207 g (0.564 mmol) PbBr<sub>2</sub>, 1.5 mL HOA, 1.5 mL OLAm and 15 mL of ODE were placed in 100 mL three neck round flask. Under vacuum, solution was constantly stirred at 110 °C for 1 hour until all PbBr<sub>2</sub> forms complexes with HOA

and OLAm. Under Argon, temperature was raised to 180 °C at which preheated 1.2 mL Cs-oleate (1.4 mmol) was swiftly injected. The reaction took place about 5 s, immediately followed by quenching with an ice bath. The resulting NCs are highly luminescent. NCs were cannula-transferred to prevent ambient exposure and then brought into the glovebox for further purification.

**Purification process of CsPbBr<sub>3</sub> NCs.** To ensure most of excess ligands, by-products, and unreacted species were removed, an extensive purification process was performed. The crude solution was centrifuged at 6k rpm for 45 min and the strongly colored supernatant is discarded. 5 mL of each methyl acetate (MeAc) and toluene were added to disperse NCs. The solution was centrifuged at 6k rpm for 15 min and the colored supernatant is discarded again. NCs were dispersed in 5 mL toluene, along with an addition of 200 μL of dried HOA and OLAm. Another 5 mL of MeAc added and the solution was centrifuged again. The less colored supernatant was discarded this time. The previous procedure was repeated once more but only with an addition of 75 μL of HOA and OLAm. After centrifuging, the supernatant was removed. The NCs were dispersed once more in 5 mL toluene, centrifuged at 3k rpm for 3 min. The final supernatant was collected and stored in the glovebox.

For gentle purification process, the crude solution was centrifuged at 6k rpm for 45 min and the supernatant was discarded. 5 mL of toluene was added once again and the solution was centrifuged at 3k rpm for 3 min. Strongly colored supernatant was collected.

**X bromide (X = OLAm<sup>+</sup>, TriBA<sup>+</sup>, DiBA<sup>+</sup>, nBA<sup>+</sup>) ligands syntheses.** 48% aqueous HBr and 10 mol % excess amine were reacted in ethanol and stirred overnight. H<sub>2</sub>O introduced from aqueous HBr was removed by the rotary evaporator. The condensed product was introduced in excess diethyl ether and placed in a freezer at -20 °C until salt was reprecipitated while unreacted amine stayed dissolved in diethyl ether. This procedure was repeated twice more to yield highest purity. The finally filtered salts were further dried in a vacuum oven at room temperature.

**X-Y ionic salt (X = OLAm<sup>+</sup>, TriBA<sup>+</sup>, DiBA<sup>+</sup>, nBA<sup>+</sup>; Y = BA<sup>-</sup>, DFA<sup>-</sup>) ligands preparation.** Ligand solutions that do not need to be directly synthesized were prepared by simple mixing. Amines and acids were placed in anhydrous toluene (in which solvent that CsPbBr<sub>3</sub> NCs are dispersed) and stirred overnight in the glovebox.

**Optical characterization.** NC solution was sealed in a 1 mm path length quartz cuvette for optical measurements. Toluene in a cuvette was taken as a blank. PerkinElmer Lambda 950S spectrophotometer was used for absorbance measurement. PTI Quantmaster 400 system was used for photoluminescence measurement. For relative PLQY measurement, fluorescein (99%, Sigma-Aldrich) dispersed in 0.1 M sodium hydroxide in ethanol was used as a standard dye. For TRPL measurement, time correlated single photon counting setup (TCSPC) was used on QM-400 system to measure lifetimes with 433 nm laser

diode as a light source. The lifetimes and their values are listed in Table S1 in Electronic Supplementary Information.

**High-resolution transmission electron microscopy (HR-TEM), and X-ray Diffraction (XRD) characterizations.** FEI Titan 80-300 TEM with 300 kV voltage was used for high-resolution TEM images. XRD was taken using a Malvern PANalytical Empyrean system with 40 kV and 40 mA.

**Molecular dynamics simulations.** Ab-initio molecular dynamics was performed to sample structures (for subsequent geometry optimization) for each of the isolated cations and ion-pairs using the Perdew-Burke-Ernzerhof (PBE) exchange-correlation form of the generalized gradient approximation (GGA).<sup>56</sup> The calculations were performed using version 5.4.4 of the Vienna Ab Initio Simulation Package (VASP).<sup>57</sup> The NVT ensemble was used with a Nose-Hoover thermostat. AIMD was performed at 373K and 0.5 fs time steps for a minimum of 2 ps. The calculations were spin-polarized with a plane-wave cut-off of 400 eV (chosen due to the presence of C, N, O, and F in some complexes), and an energy convergence criterion of  $10^{-4}$  eV, and we considered only the  $\Gamma$  point for sampling the first Brillouin zone. For OLAm<sup>+</sup>, 22 Å of vacuum was added in all directions, 18 Å for TriBAm<sup>+</sup>, and 16 Å for DiBAm<sup>+</sup>. The five minimum energy structures, spaced apart by at least 50 fs, were visually compared, and the lowest energy structures with unique conformations were selected for subsequent geometry optimizations. We emphasize that the sole purpose of the planewave AIMD simulations was to sample structures that were then optimized per the method described below.

**B3LYP calculations.** Individual ion structures and the selected ion-pair structures were optimized using B3LYP/ aug-cc-pvtz and the Gaussian software.<sup>58</sup> The structures were optimized with 'tight' convergence, to a root mean square force of  $5.1 \times 10^{-4}$  eV/Å and max force of  $7.7 \times 10^{-4}$  eV/Å, and a root mean square displacement of  $2.1 \times 10^{-5}$  Å and a maximum displacement of  $3.2 \times 10^{-5}$  Å. We chose B3LYP for its reasonable performance for covalent and non-covalent interactions of small molecules.<sup>59</sup> To test the effect of our choice of computational method on ion pair energetics, we also performed calculations using B3LYP/ aug-cc-pvtz and the D3 dispersion correction with Becke-Johnson dampening (D3(BJ)),<sup>60</sup> and the  $\omega$ B97X-D hybrid-exchange functional,<sup>61</sup> and MP2<sup>62</sup> calculations for select ion pairs. We found that the trend in energies with respect to the identity of the anion remained the same (Table S3-S5 in Electronic Supplementary Information) across all methods tested. All structure files from final optimized geometries are attached in the *Ionic pairs molecular structure* attachment file.

## Results and discussion

### NCs synthesis and characterization

For this study, it is beneficial to prepare NCs with a minimum number of native surface ligands while still keeping NCs colloidal stable. This is to more clearly elucidate the interactions between the ligand species of interest and the NC surface. Indeed, NCs with *gentle* purification processes (see

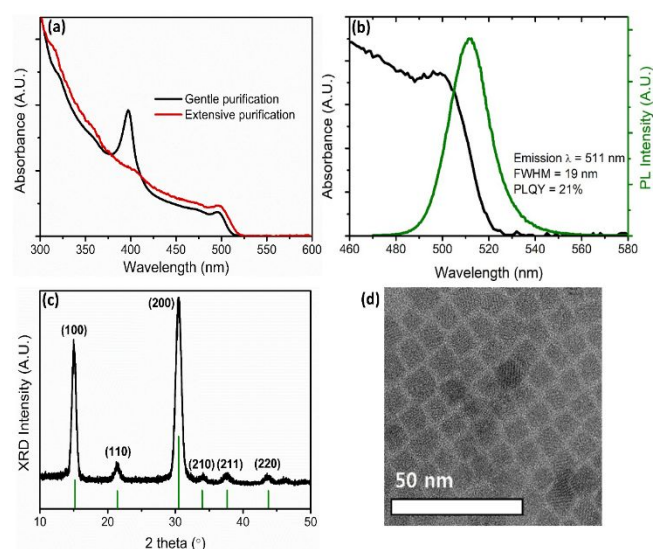


Figure 1. (a) Absorbance spectra of two differently purified CsPbBr<sub>3</sub> NCs with (OLAm<sup>+</sup>)(Br) treatment. NCs prepared with gentle purification show a peak at around 390 nm upon ligand treatment, indicating a formation of other complex species. (b) Absorbance and PL spectra of CsPbBr<sub>3</sub>. (c) XRD patterns indicating cubic phase of CsPbBr<sub>3</sub> NCs (d) TEM image showing an average NC size of  $7.9 \pm 1.4$  nm.

Purification process of CsPbBr<sub>3</sub> NCs in Experimental section) showed complications upon ligand treatment likely due to significant amount of various species including Pb-oleate, unreacted species, and excess native ligands such as OLAm and HOA. As shown in Figure 1a, ligand treated NCs with *gentle* purification show a peak in light absorbance at around 390 nm. The peak is at much lower wavelength than 503 nm, the first excitonic absorption peak of CsPbBr<sub>3</sub> NCs. This is likely due to light absorption by MHP precursor complexes, formed between unreacted precursor and ligands, that are much smaller than the size of NCs. NCs with the *extensive* purification process demonstrate consistent absorbance spectra with no additional peaks, suggesting that they have cleaner surface system for our ligand – surface interaction study. Therefore, for this study, control (as-synthesized) NCs were placed under *extensive* purification processes to remove the excess ligands and unreacted species.

Figure 1 provides characterization results of the extensively purified NCs prior to ligand treatment. Figure 1b features absorbance and PL spectra. The PL peak is located at 511 nm with FWHM of 19 nm. The relatively low PLQY value of 21% compared to the values typically reported in the literature<sup>31, 53</sup> is due to removal of native ligands as much as possible during the extensive purification step. Figure 1c displays X-ray diffraction (XRD) peaks at 16° and 32° corresponding to strong orientations of (100) and (200) planes parallel to the substrate, respectively. The peaks of (110) at 22°, (210) at 34°, (211) at 37° and (220) at 44° are also in a good agreement with CsPbBr<sub>3</sub> without any detectable presence of impurities.<sup>26</sup> Based on transmission electronic microscope (TEM) images (Figure 1d), the average size of NCs is measured to be  $7.9 \pm 1.4$  nm which is consistent with the absorbance and PL peak wavelengths.<sup>63</sup> These characterization results confirm that CsPbBr<sub>3</sub> NCs were successfully prepared as the base system for ligand treatment study.

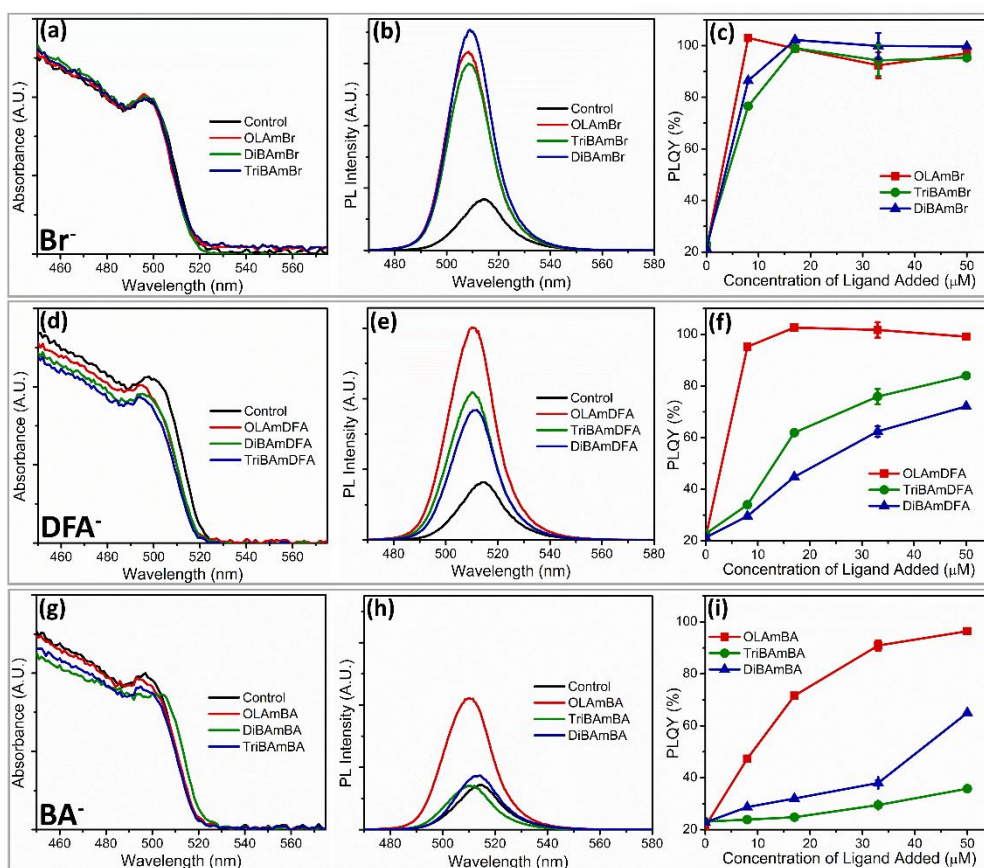


Figure 2. (a, d, h) Absorbance spectra of NCs treated with 33  $\mu\text{M}$  of various cation – anion pairs. Each row represents the data from a set of various salt with the same anion. (b, e, h) PL spectra of the corresponding samples. Varying degrees of PL intensity with respect to that of untreated control NCs is observed depending on the combination of anion and cation. (c, f, i) PLQYs as a function of concentration of ligand treated on NCs show a clear dependence on each cation and anion.

A study by Nenon *et al.*<sup>53</sup> suggests that the interaction between the anion of an ionic salt and under-coordinated  $\text{Pb}^{2+}$  plays a significant role in passivation efficacy. Particularly, the degree of match between the Lewis basicity of the anion and the soft Lewis acid  $\text{Pb}^{2+}$  sites seems to be a major factor in charge trap passivation efficacy on  $\text{CsPbBr}_3$  NC surface. Based on those findings, we selected a range of anions with various Lewis basicity that previously showed widely different degrees of trap passivation: bromide ( $\text{Br}^-$ ), difluoroacetate ( $\text{DFA}^-$ ), and benzoate ( $\text{BA}^-$ ). A set of cations was chosen to yield various interaction energies when paired with the anions: oleylammonium ( $\text{OLAm}^+$ ), n-butylammonium ( $\text{nBAm}^+$ ), dibutylammonium ( $\text{DiBAm}^+$ ), tributylammonium ( $\text{TriBAm}^+$ ), tetrabutylammonium ( $\text{TeBAm}^+$ ). Cations with differing numbers of carbon chains were selected to alter the electron density around nitrogen of cation, and thus its binding strength with the anions. Each cation and anion were matched to form total of 15 pairs of ionic salts to study their effect on trap passivation in  $\text{CsPbBr}_3$  NCs.

#### PLQY results

The absorbance, PL, and PLQY results of NCs treated with various cation – anion pairs are displayed in Figure 2. Absorbance spectra in Figure 2a, d, and g show relatively minimal shifts and changes in magnitude, indicating a negligible change in energy levels and population of NCs in the solution due to ligand treatment. However, their PL spectra show

significant variations in intensities depending on specific combination of cation and anion (Figure 2b, e, and h). Our PL results suggest that a degree of trap passivation strongly depends on both cation and anion of choice. In the case of the  $\text{Br}^-$  anion set, all treatment with  $\text{OLAm}^+$ ,  $\text{DiBAm}^+$ , and  $\text{TriBAm}^+$  pairs resulted in superb passivation, yielding PLQY values of over 95%. In other words, there is no appreciable dependence of PLQY on the cation when paired with the  $\text{Br}^-$  anion. These results imply that, first, the extra  $\text{Br}^-$  anions from the introduced ionic salt effectively fill in the  $\text{Br}^-$  vacancies on  $\text{CsPbBr}_3$  NC surface. Second, the interaction energy of all cation –  $\text{Br}^-$  pairs may be low such that sufficient amount of charged X-type ligands successfully passivates detrimental defects. Lastly, all  $\text{OLAm}^+$ ,  $\text{DiBAm}^+$ , and  $\text{TriBAm}^+$  cations do not inherently possess compatibility issues such as steric hindrance with  $\text{CsPbBr}_3$  NC surface.

$\text{DFA}^-$  has been recently discovered as a promising charge trap passivating anion for  $\text{Br}^-$  vacancy on  $\text{CsPbBr}_3$  NC surface.<sup>53</sup> Based on energy level calculations, PLQY, and  $^1\text{H}$ -nuclear magnetic resonance (NMR) results, Nenon *et al.*<sup>53</sup>, found that the soft Lewis basicity of  $\text{DFA}^-$  matches well with soft Lewis acidity of  $\text{Pb}^{2+}$  and can serve as an effective trap passivating agent.<sup>53</sup> Our results also show that  $\text{DFA}^-$ , when paired with  $\text{OLAm}^+$ , show superior passivation (Figure 2f). However, interestingly, we found that the passivation efficacy drastically decreases when

DFA<sup>-</sup> is paired with DiBAm<sup>+</sup> and TriBAm<sup>+</sup>. Treatment with (DiBAm<sup>+</sup>)(DFA<sup>-</sup>) yielded at most 80% PLQY while treatment with (TriBAm<sup>+</sup>)(DFA<sup>-</sup>) produced an even lower PLQY (~70%). This observation of a large variation in PLQY from ~70% to ~100% observed in DFA<sup>-</sup> set with various cation pairs strongly suggests that the charge trap passivation efficacy of ionic salts is significantly impacted by the pairing with cation. Our results show that, although DFA<sup>-</sup> can be an effective passivating anion, it is not as competent as Br<sup>-</sup>, especially when paired with cations other than OLAm<sup>+</sup>. The difference in passivation efficacy of each anion is possibly explained by the variation in their interaction with their cation counterpart.

The third anion used in testing, BA<sup>-</sup>, has softer Lewis basicity than DFA<sup>-</sup> and is expected to be superior for Pb<sup>2+</sup> coordination according to the study by Nenon *et al.*<sup>53</sup> However, the study<sup>53</sup> showed that BA<sup>-</sup> may not be as effective passivating ligand. In this study, we found that BA<sup>-</sup> can effectively passivate charge traps depending on the choice of cations. The (OLAm<sup>+</sup>)(BA<sup>-</sup>) pair yielded superior passivation with ~90% PLQY while the (DiBAm<sup>+</sup>)(BA<sup>-</sup>) and (TriBAm<sup>+</sup>)(BA<sup>-</sup>) pairs showed relatively low PLQYs of 60% and 30%, respectively. Similar with the DFA<sup>-</sup> set, the results from the BA<sup>-</sup> set also shows ionic pairing dependent PLQY variations. Overall, the BA<sup>-</sup> pairs were found to be not as effective for passivation compared to DFA<sup>-</sup> pairs, which is consistent with the results in Nenon *et al.*<sup>53</sup> Though this may be explained by the large size of the benzoate anion causing steric hindrance, we propose that the interaction strengths of the cation – BA<sup>-</sup> pairs may be larger than those of cation – DFA<sup>-</sup> or Br<sup>-</sup> pairs, hindering their ability to dissociate and ultimately passivate trap sites.

We note that the nBAm<sup>+</sup> and TeBAm<sup>+</sup> cations, regardless of anions they were paired with, behaved very differently from DiBAm<sup>+</sup>, TriBAm<sup>+</sup>, and OLAm<sup>+</sup>. Absorbance spectra of NCs treated with (nBAm<sup>+</sup>)(Br<sup>-</sup>) and (TeBAm<sup>+</sup>)(Br<sup>-</sup>) in Figure S1 (Electronic Supplementary Information) feature a significant decrease in absorption intensity of the entire spectra, but especially the first excitonic peaks at 503 nm. These results suggest that all pairs with nBAm<sup>+</sup> and TeBAm<sup>+</sup> cations that we used cause degradation of NCs. Due to this complication, further studies with nBAm<sup>+</sup> and TeBAm<sup>+</sup> sets were not pursued.

#### NC size and PL lifetime measurement

To check for a possibility that PLQY variation results shown in Figure 2 was caused by change in defect density through structural reconfiguration or deformation of NCs due to ligand treatment, we obtained TEM images of the NCs before and after the ligand treatments. For the measurements, the samples were prepared with the highest molar ratio of NCs and ligands that were used for PLQY measurements shown in Figure 2. OLAm<sup>+</sup> was selected as the cation for the measurements due to the most drastic PLQY results with paired with the various anions. The average sizes of NCs determined from the TEM images displayed in Figure 3a-c are  $7.8 \pm 1.1$  nm,  $7.9 \pm 1.2$  nm, and  $7.4 \pm 1.2$  nm for NCs treated with (OLAm<sup>+</sup>)(Br<sup>-</sup>), (OLAm<sup>+</sup>)(BA<sup>-</sup>), and (OLAm<sup>+</sup>)(DFA<sup>-</sup>) respectively. The average values of all samples fall within the statistical variation when compared to the as-synthesized NCs. Also, there were no significant changes

to shapes of NCs. These results indicate that the ligand treatment-induced structural changes are statistically insignificant and not likely to be responsible for the observed differences in PLQY shown in Figure 2.

To better understand the origin of different PLQY values with various cation – anion pair treatment, we performed time-resolved photoluminescence (TRPL) measurements. A comparison of PL lifetimes allows us to gauge relative differences in a degree of non-radiative recombination that is primarily caused by charge trap states. Average lifetimes of NCs treated with cation – Br<sup>-</sup> pairs, which yielded >95% PLQY (Figure 2c), are measured to be at least 2.5 times longer compared to

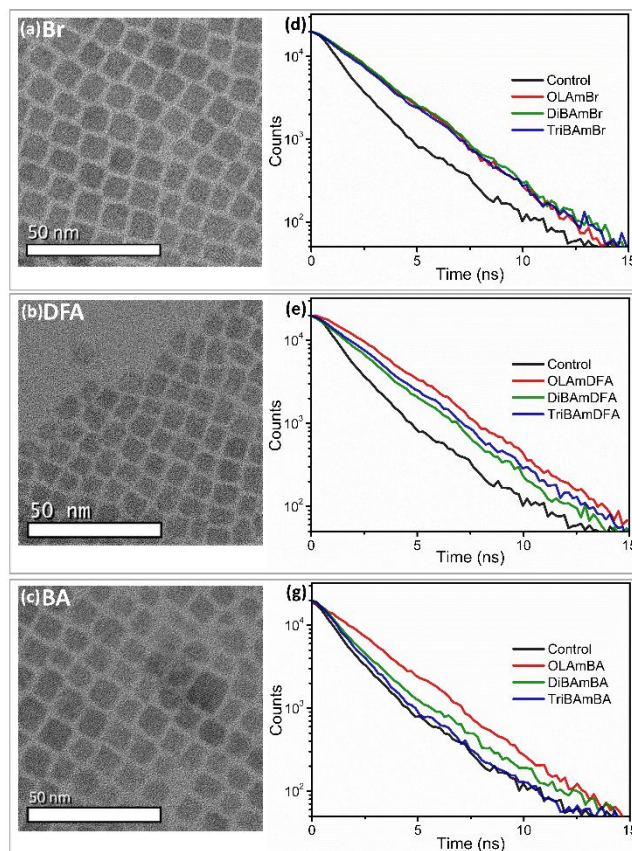


Figure 3. TEM images of NCs treated with the highest molar ratio of (a) OLAmBr, (b) OLAmDFA and (c) OLAmBA used for PLQY measurements. No significant structural change is observed. PL lifetime measurements of control (untreated) NCs versus NCs treated with various cations (OLAm<sup>+</sup>, DiBAm<sup>+</sup>, TriBAm<sup>+</sup>) paired with (d) Br<sup>-</sup>, (e) DFA<sup>-</sup>, and (f) BA<sup>-</sup>.

those of untreated NCs (Figure 3d and Table S1). The trend in PL lifetime is also successfully reflected in cation-dependent PLQY results in DFA<sup>-</sup> and BA<sup>-</sup> sets. In DFA<sup>-</sup> set, (OLAm<sup>+</sup>)(DFA<sup>-</sup>) yielded the longest lifetime, followed by (TriBAm<sup>+</sup>)(DFA<sup>-</sup>) and then (DiBAm<sup>+</sup>)(DFA<sup>-</sup>). BA<sup>-</sup> set showed the least increase of lifetime, as predicted in PLQY; highest lifetime from (OLAm<sup>+</sup>)(BA<sup>-</sup>), followed by (DiBAm<sup>+</sup>)(BA<sup>-</sup>) and (TriBAm<sup>+</sup>)(BA<sup>-</sup>). The PL lifetime values are provided in Table S1 in Electronic Supplementary Information. As a result, the PL lifetime results suggest that increase in PLQY upon ligand treatment is due to reduction in non-radiative recombination which largely depends on the combination of cation – anion pairs.

#### DFT calculations and analysis

To test our hypothesis that interaction energies of ion pairs are a major factor in determining charge trap passivation efficacy, DFT calculations were performed. Initial ionic pair structures were found using *ab initio* molecular dynamics trajectories (details provided in Experimental section: Molecular Dynamics Simulations), and structures were then subsequently optimized with the B3LYP/aug-cc-pvtz functional and basis set. Simulations were conducted in the absence of a solvent, full calculation details are provided in Experimental section: B3LYP Calculations and all DFT – optimized molecular structures are provided in *Ionic pairs molecular structure* file attachment. Additionally, images of the ion pair structures are provided in the Electronic Supplementary Information, Figure S2. The reaction between the cations and anions is not purely electrostatic for all complexes. Optimization of the DFA<sup>-</sup> and BA<sup>-</sup> ion pairs result in transfer of a proton from the cation to the anion (forming two approximately neutral molecules) for all pairs except (TriBAm<sup>+</sup>)(DFA<sup>-</sup>) where we found retention of the proton by TriBAm<sup>+</sup> to be slightly (2 kJ/mol) more favorable (Figure S2). We do not observe proton transfer for the Br<sup>-</sup> pairs. The interaction energy was calculated using the B3LYP/aug-cc-pvtz energies for ion pairs and individual ions and cations as:

$$\Delta E_{\text{inter.}} = E_{\text{AB}} - E_{\text{A}^+} - E_{\text{B}^-} \quad (1)$$

More exothermic interaction energy values indicate that the cation-anion pair is in a more stable and energetically favorable state. Conversely, the less exothermic the interaction energy is, the more likely the pair is to dissociate into the free ion species. Figure 4 reports the DFT results (values displayed in Table S2 in Electronic Supplementary Information); the trend in calculated interaction energies of ionic pairs is generally consistent with the PLQY results, as discussed below.

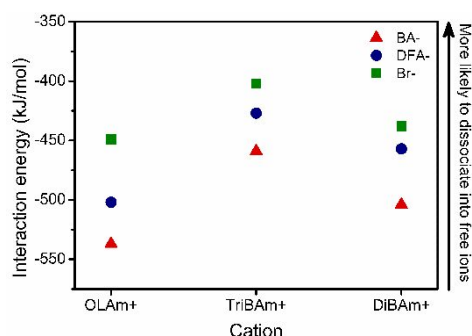


Figure 4. Interaction energies of various ionic pairs. Lower negative interaction energy is related to a higher tendency of the ionic pair dissociating into free ion species.

Among the ionic pairs, cation – BA<sup>-</sup> pairs show the most exothermic interaction energies overall; they have the highest tendency to stay as an ionic pair and are expected to show the least effective trap passivation. Cation – DFA<sup>-</sup> pairs have the second highest tendency to stay as a pair while the cation – Br<sup>-</sup> pairs have the lowest. The calculation results closely resemble our PLQY results, in which overall cation – BA<sup>-</sup> pairs yielded lower PLQY ranging from 30 to 90%, followed by cation – DFA<sup>-</sup> pairs from 70 to 100% and cation – Br<sup>-</sup> from 95% to 100%. The interaction energy values among the set of ionic pairs with the same cation show a strong correlation with the trend observed in the PLQY results. For example, the interaction energy of

(TriBAm<sup>+</sup>)(Br<sup>-</sup>) is the least exothermic (-400 kJ/mol) followed by (TriBAm<sup>+</sup>)(DFA<sup>-</sup>) with -430 kJ/mol and (TriBAm<sup>+</sup>)(BA<sup>-</sup>) with -460 kJ/mol while their respective PLQY (highest) values are 100%, 84%, and 36%. Similarly, the interaction energy values of (DiBAm<sup>+</sup>)(Br<sup>-</sup>) (-440 kJ/mol), (DiBAm<sup>+</sup>)(DFA<sup>-</sup>) (-460 kJ/mol), and (DiBAm<sup>+</sup>)(BA<sup>-</sup>) (-500 kJ/mol) are in a good agreement with the trend of their PLQY values (100%, 72% and 65%, respectively). OLAm<sup>+</sup> – anion pairs also show similar results, with the exception of passivation by (OLAm<sup>+</sup>)(DFA<sup>-</sup>), which is as superior as (OLAm<sup>+</sup>)(Br<sup>-</sup>) despite its 50 kJ/mol more exothermic interaction energy. Additionally, our observation of all cation – Br<sup>-</sup> pairs yielding superior passivation is consistent with their more endothermic interactions energies relative to cation – DFA<sup>-</sup> and cation – BA<sup>-</sup> pairs. With respect to the cation identity, no discernable trend between PLQY results and DFT results was observed amongst the cations studied in this study.

Our results suggest that interaction energy of an ionic pair may impose a considerable impact on the trap passivation efficacy. However, it is precarious to conclude that the interaction energy of an ionic pair is the only major factor governing the trap passivation efficacy. It is one of many factors that can contribute to the overall passivation mechanism such as the interaction of ions with MHP NC surfaces, the interaction with the native ligands, the entropic effects on the system, etc. In addition, we emphasize that the chemical properties of the anions, such as Lewis basicity,<sup>53</sup> is also very important as they govern the direct interaction between the anions and the exposed Pb<sup>2+</sup> atoms. Therefore, our DFT results can not entirely account for our experimental results, as evidenced in the absence of a trend between cations in comparison to the experimental data. However, a general correlation of our DFT results with the PLQY results is a strong indication that the interaction energy of cation-anion pair is a considerable factor in determining the passivation efficacy of the ionic pair.

Here it should be noted that our results may help explain the peculiar behavior of BA<sup>-</sup> as an ineffective trap passivating anion that was previously observed in the literature.<sup>53</sup> The soft Lewis base BA<sup>-</sup> was initially thought to be well-matched for coordination with soft Lewis acid Pb<sup>2+</sup>. However, experimental results showed that using BA<sup>-</sup> resulted in poor charge trap passivation. The authors speculated that the steric hindrance due to bulky benzene ring may be the cause.<sup>53</sup> Our results in this work suggest that another important factor that can explain this peculiarity is the lower tendency of cation-BA<sup>-</sup> pairs to dissociate into ionic species compared to other cation-anion pairs.

Based on the findings from this work, ideal ionic pairs can be selected by carefully considering several factors. As supported by a previous study<sup>53</sup> and our results, the affinity of an anion to coordinate with exposed Pb<sup>2+</sup> is an important factor to consider. The anion should be chosen to have soft Lewis basicity to match the soft Lewis acidity of the under-coordinated Pb<sup>2+</sup> atoms on the surface, without any major steric hindrance. Additionally, as we have demonstrated in this work, it is beneficial to select an anion – cation pair with relatively low interaction energy. Therefore, the choice of cation should be carefully considered

as it imposes a considerable influence on passivation mechanism as well.

Interaction energy between the cation and anion of an ionic salt can be exploited as a key factor for a facile and rapid screening platform for an optimal ligand selection. In the process of selecting a range of ionic salts for NC surface treatments, conducting numerous ligand treatment tests demands a large amount of time, cost and effort. However, an initial screening of ligand candidates by using the cation – anion interaction energy as a variable can significantly reduce the number of physical tests that need to be completed. It also substantially increases a range of ligands to be screened, which elevates the chance of finding a novel and effective ligand. This screening process is readily applicable for defect passivation of other perovskite-based NCs, and therefore bulk thin film compositions, as NCs have been shown to be an excellent model system for studying surface passivation treatments for bulk thin films.<sup>48</sup> For instance, it could be greatly beneficial for CsPbCl<sub>3</sub> and CsPbI<sub>3</sub> NC compositions, which have demonstrated low stabilities and challenges for PLQY improvement.<sup>25</sup> Low stability causes inevitable difficulties on experimental testing such as NC batch variability and a limited number of ligands for treatment. A wide range of computational screening of various ionic pairs may save time and cost caused by such complexities and help finding optimal ligands for effective surface defect passivation on MHP NCs.

## Conclusions

In this work, we studied the impact of various cation – anion pairs on CsPbBr<sub>3</sub> surface trap passivation. Collective findings from PLQY, TEM and lifetime results show that a degree of trap passivation is not only determined by the compatibility of anion in ionic pair to passivate Br<sup>-</sup> vacancies, but also the choice of cation that is paired with. Although it is hard to elucidate how cation partakes in trap passivation mechanism, our work suggests that one of the governing factors to the passivation efficacy is the nature of ionic pairing, or particularly, interaction energy of cation – anion pair. The implication of this work for applications suggests that the interaction energy between cation – anion pairs needs to be taken into account when selecting ideal ligand for surface trap passivation on MHP NCs.

## Conflicts of interest

There are no conflicts to declare.

## Acknowledgements

This work is supported by the National Science Foundation under Grant No. DMR-2003978. This material is based upon work supported, in part, by the National Science Foundation under Grant No. CBET-1752048. Any opinions, findings, and conclusions or recommendations expressed in this material are those of the authors and do not necessarily reflect the views of the National Science Foundation. The authors acknowledge

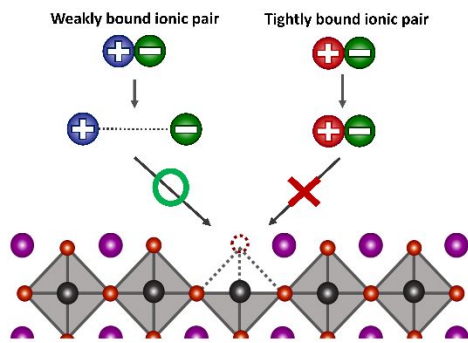
Research Computing at The University of Virginia for providing computational resources and technical support that have contributed to the results reported within this publication. URL: <https://rc.virginia.edu>.

## Reference

1. Y. Fu, H. Zhu, J. Chen, M. P. Hautzinger, X. Y. Zhu and S. Jin, *Nature Reviews Materials*, 2019, **4**, 169-188.
2. J. Sun, J. Wu, X. Tong, F. Lin, Y. Wang and Z. M. Wang, *Advanced Science*, 2018, **5**, 1700780.
3. S. Bai, Z. Yuan and F. Gao, *Journal of Materials Chemistry C*, 2016, **4**, 3898-3904.
4. Z. Song, S. C. Wathage, A. B. Phillips and M. J. Heben, *Journal of Photonics for Energy*, 2016, **6**, 022001.
5. H. Dong, C. Zhang, X. Liu, J. Yao and Y. S. Zhao, *Chemical Society Reviews*, 2020, **49**, 951-982.
6. Y. Dong, Y. Zou, J. Song, X. Song and H. Zeng, *Journal of Materials Chemistry C*, 2017, **5**, 11369-11394.
7. X. Di, L. Shen, J. Jiang, M. He, Y. Cheng, L. Zhou, X. Liang and W. Xiang, *Journal of Alloys and Compounds*, 2017, **729**, 526-532.
8. Y.-H. Kim, H. Cho and T.-W. Lee, *PNAS*, 2016, **113**, 11694-11702.
9. G. Li, F. W. R. Rivarola, N. J. L. K. Davis, S. Bai, T. C. Jellicoe, F. d. I. Peña, S. Hou, C. Ducati, F. Gao, R. H. Friend, N. C. Greenham and Z.-K. Tan, *Advanced Materials*, 2016, **28**, 3528-3534.
10. A. Perumal, S. Shendre, M. Li, Y. K. E. Tay, V. K. Sharma, S. Chen, Z. Wei, Q. Liu, Y. Gao, P. J. S. Buenconsejo, S. T. Tan, C. L. Gan, Q. Xiong, T. C. Sum and H. V. Demir, *Scientific Reports*, 2016, **6**, 1-10.
11. N. Wang, L. Cheng, R. Ge, S. Zhang, Y. Miao, W. Zou, C. Yi, Y. Sun, Y. Cao, R. Yang, Y. Wei, Q. Guo, Y. Ke, M. Yu, Y. Jin, Y. Liu, Q. Ding, D. Di, L. Yang, G. Xing, H. Tian, C. Jin, F. Gao, R. H. Friend, J. Wang and W. Huang, *Nature Photonics*, 2016, **10**, 699-704.
12. Z. Xiao, R. A. Kerner, L. Zhao, N. L. Tran, K. M. Lee, T.-W. Koh, G. D. Scholes and B. P. Rand, *Nature Photonics*, 2017, **11**, 108-115.
13. F. Yan, J. Xing, G. Xing, L. Quan, S. T. Tan, J. Zhao, R. Su, L. Zhang, S. Chen, Y. Zhao, A. Huan, E. H. Sargent, Q. Xiong and H. V. Demir, *Nano Lett.*, 2018, **18**, 3157-3164.
14. X. Zhang, H. Lin, H. Huang, C. Reckmeier, Y. Zhang, W. C. H. Choy and A. L. Rogach, *Nano Lett.*, 2016, **16**, 1415-1420.
15. X. Zhang, C. Sun, Y. Zhang, H. Wu, C. Ji, Y. Chuai, P. Wang, S. Wen, C. Zhang and W. W. Yu, *J. Phys. Chem. Lett.*, 2016, **7**, 4602-4610.
16. H. Guan, S. Zhao, H. Wang, D. Yan, M. Wang and Z. Zang, *Nano Energy*, 2020, **67**, 104279.
17. X. Li, Y. Wu, S. Zhang, B. Cai, Y. Gu, J. Song and H. Zeng, *Advanced Functional Materials*, 2016, **26**, 2435-2445.
18. Q. Mo, T. Shi, W. Cai, S. Zhao, D. Yan, J. Du and Z. Zang, *Photonics Research*, 2020, **8**, 1605.
19. S. Zhao, Y. Zhang and Z. Zang, *Chem Commun (Camb)*, 2020, **56**, 5811-5814.
20. R. E. Beal, D. J. Slotcavage, T. Leijtens, A. R. Bowring, R. A. Belisle, W. H. Nguyen, G. F. Burkhard, E. T. Hoke and M. D. McGehee, *J. Phys. Chem. Lett.*, 2016, **7**, 746-751.

21. M. Kulbak, S. Gupta, N. Kedem, I. Levine, T. Bendikov, G. Hodes and D. Cahen, *J. Phys. Chem. Lett.*, 2016, **7**, 167-172.
22. J.-F. Liao, H.-S. Rao, B.-X. Chen, D.-B. Kuang and C.-Y. Su, *J. Mater. Chem. A*, 2017, **5**, 2066-2072.
23. R. J. Sutton, G. E. Eperon, L. Miranda, E. S. Parrott, B. A. Kamino, J. B. Patel, M. T. Hörantner, M. B. Johnston, A. A. Haghighirad, D. T. Moore and H. J. Snaith, *Advanced Energy Materials*, 2016, **6**, 1502458.
24. Q. A. Akkerman, V. D'Innocenzo, S. Accornero, A. Scarpellini, A. Petrozza, M. Prato and L. Manna, *J. Am. Chem. Soc.*, 2015, **137**, 10276-10281.
25. G. Nedelcu, L. Protesescu, S. Yakunin, M. I. Bodnarchuk, M. J. Grotevent and M. V. Kovalenko, *Nano Lett.*, 2015, **15**, 5635-5640.
26. D. Parobek, Y. Dong, T. Qiao, D. Rossi and D. H. Son, *J. Am. Chem. Soc.*, 2017, **139**, 4358-4361.
27. Y. Tong, E. Bladt, M. F. Aygüler, A. Manzi, K. Z. Milowska, V. A. Hintermayr, P. Docampo, S. Bals, A. S. Urban, L. Polavarapu and J. Feldmann, *Angewandte Chemie International Edition*, 2016, **55**, 13887-13892.
28. D. Yan, S. Zhao, H. Wang and Z. Zang, *Photonics Research*, 2020, **8**, 1086.
29. F. Di Stasio, S. Christodoulou, N. Huo and G. Konstantatos, *Chemistry of Materials*, 2017, **29**, 7663-7667.
30. G. Li, J. Huang, H. Zhu, Y. Li, J.-X. Tang and Y. Jiang, *Chemistry of Materials*, 2018, **30**, 6099-6107.
31. J. De Roo, M. Ibanez, P. Geiregat, G. Nedelcu, W. Walravens, J. Maes, J. C. Martins, I. Van Driessche, M. V. Kovalenko and Z. Hens, *ACS Nano*, 2016, **10**, 2071-2081.
32. J. Song, T. Fang, J. Li, L. Xu, F. Zhang, B. Han, Q. Shan and H. Zeng, *Advanced Materials*, 2018, **30**, 1805409.
33. L. M. Herz, *Annual Review of Physical Chemistry*, 2016, **67**, 65-89.
34. M. B. Johnston and L. M. Herz, *Acc. Chem. Res.*, 2016, **49**, 146-154.
35. M. Stolterfoht, C. M. Wolff, J. A. Márquez, S. Zhang, C. J. Hages, D. Rothhardt, S. Albrecht, P. L. Burn, P. Meredith, T. Unold and D. Neher, *Nature Energy*, 2018, **3**, 847-854.
36. S. D. Stranks, *ACS Energy Lett.*, 2017, **2**, 1515-1525.
37. S. D. Stranks, V. M. Burlakov, T. Leijtens, J. M. Ball, A. Goriely and H. J. Snaith, *Phys. Rev. Applied*, 2014, **2**, 034007.
38. W. Tress, N. Marinova, O. Inganäs, M. K. Nazeeruddin, S. M. Zakeeruddin and M. Graetzel, *Advanced Energy Materials*, 2015, **5**, 1400812.
39. G.-J. A. H. Wetzelaer, M. Scheepers, A. M. Sempere, C. Momblona, J. Ávila and H. J. Bolink, *Advanced Materials*, 2015, **27**, 1837-1841.
40. Q. Chen, H. Zhou, T.-B. Song, S. Luo, Z. Hong, H.-S. Duan, L. Dou, Y. Liu and Y. Yang, *Nano Lett.*, 2014, **14**, 4158-4163.
41. B. A. Koscher, J. K. Swabeck, N. D. Bronstein and A. P. Alivisatos, *J. Am. Chem. Soc.*, 2017, **139**, 6566-6569.
42. N. K. Noel, A. Abate, S. D. Stranks, E. S. Parrott, V. M. Burlakov, A. Goriely and H. J. Snaith, *ACS Nano*, 2014, **8**, 9815-9821.
43. J. Pan, Y. Shang, J. Yin, M. De Bastiani, W. Peng, I. Dursun, L. Sinatra, A. M. El-Zohry, M. N. Hedhili, A.-H. Emwas, O. F. Mohammed, Z. Ning and O. M. Bakr, *J. Am. Chem. Soc.*, 2018, **140**, 562-565.
44. H. Wu, Y. Zhang, M. Lu, X. Zhang, C. Sun, T. Zhang, V. L. Colvin and W. W. Yu, *Nanoscale*, 2018, **10**, 4173-4178.
45. D. Yang, X. Li and H. Zeng, *Advanced Materials Interfaces*, 2018, **5**, 1701662.
46. H. Zhang, M. K. Nazeeruddin and W. C. H. Choy, *Advanced Materials*, 2019, **31**, 1805702.
47. X. Zheng, B. Chen, J. Dai, Y. Fang, Y. Bai, Y. Lin, H. Wei, X. C. Zeng and J. Huang, *Nature Energy*, 2017, **2**, 1-9.
48. M. R. Alpert, J. S. Niezgodá, A. Z. Chen, B. J. Foley, S. Cuthriell, L. U. Yoon and J. J. Choi, *Chemistry of Materials*, 2018, **30**, 4515-4526.
49. T. Chiba, Y. Hayashi, H. Ebe, K. Hoshi, J. Sato, S. Sato, Y.-J. Pu, S. Ohisa and J. Kido, *Nature Photonics*, 2018, **12**, 681-687.
50. Y. Wang, T. Zhang, M. Kan and Y. Zhao, *J. Am. Chem. Soc.*, 2018, **140**, 12345-12348.
51. T. Zhao, C.-C. Chueh, Q. Chen, A. Rajagopal and A. K. Y. Jen, *ACS Energy Lett.*, 2016, **1**, 757-763.
52. X. Zheng, B. Chen, J. Dai, Y. Fang, Y. Bai, Y. Lin, H. Wei, Xiao C. Zeng and J. Huang, *Nature Energy*, 2017, **2**, 17102.
53. D. P. Nenon, K. Pressler, J. Kang, B. A. Koscher, J. H. Olshansky, W. T. Osowiecki, M. A. Koc, L.-W. Wang and A. P. Alivisatos, *J. Am. Chem. Soc.*, 2018, **140**, 17760-17772.
54. J. Kang and L.-W. Wang, *J. Phys. Chem. Lett.*, 2017, **8**, 489-493.
55. H. Uratani and K. Yamashita, *J. Phys. Chem. Lett.*, 2017, **8**, 742-746.
56. J. P. Pedew and Y. Wang, *Phys Rev B Condens Matter*, 1992, **45**, 13244-13249.
57. G. Kresse, Furthmüller, J. , *Physical Review B*, 1996, **54**.
58. M. Frisch, G. Trucks, H. B. Schlegel, G. E. Scuseria, M. A. Robb, J. R. Cheeseman, G. Scalmani, V. Barone, B. Mennucci and G. Petersson, *Inc., Wallingford CT*, 2009, **201**.
59. L. Goerigk, A. Hansen, C. Bauer, S. Ehrlich, A. Najibi and S. Grimme, *Physical Chemistry Chemical Physics*, 2017, **19**, 32184-32215.
60. S. Grimme, S. Ehrlich and L. Goerigk, *Journal of computational chemistry*, 2011, **32**, 1456-1465.
61. J.-D. Chai and M. Head-Gordon, *Physical Chemistry Chemical Physics*, 2008, **10**, 6615-6620.
62. M. J. Frisch, M. Head-Gordon and J. A. Pople, *Chemical Physics Letters*, 1990, **166**, 275-280.
63. J. Maes, L. Balcaen, E. Drijvers, Q. Zhao, J. De Roo, A. Vantomme, F. Vanhaecke, P. Geiregat and Z. Hens, *The journal of physical chemistry letters*, 2018, **9**, 3093-3097.

## TOC



Binding strength between cation and anion in a ligand has a major impact on their charge trap passivation efficacy